Understanding Selectivity of Mesoporous Silica-Grafted Diglycolamide-Type Ligands in the Solid-Phase Extraction of Rare Earths

ACS APPLIED MATERIALS & INTERFACES

www.acsami.org

Research Article

Understanding Selectivity of Mesoporous Silica-Grafted Diglycolamide-Type Ligands in the Solid-Phase Extraction of Rare Earths

Justyna Florek,* Dominic Larivière, Hanspeter Kählig, Sonia L. Fiorilli, Barbara Onida, Frédéric-Georges Fontaine, and Freddy Kleitz

Cite This: *ACS Appl. Mater. Interfaces* 2020, 12, 57003−57016

Read Online

ACCESS | Metrics & More | Article Recommendations | Supporting Information

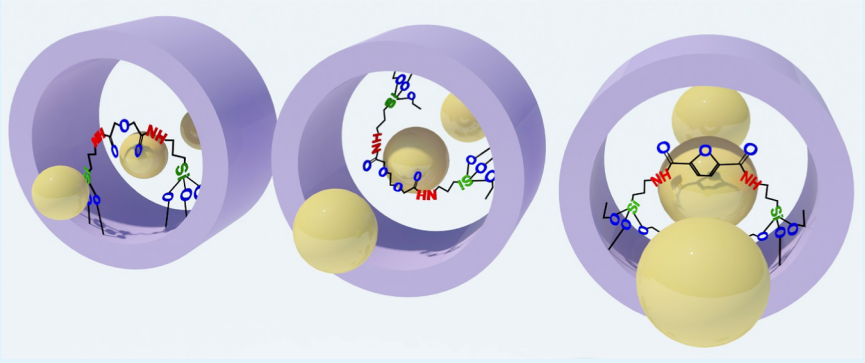

ABSTRACT: Rare earth elements (REEs) and their compounds are essential for rapidly developing modern technologies. These materials are especially critical in the area of green/sustainable energy; however, only very high-purity fractions are appropriate for these applications. Yet, achieving efficient REE separation and purification in an economically and environmentally effective way remains a challenge. Moreover, current extraction technologies often generate large amounts of undesirable wastes. In that perspective, the development of selective, reusable, and extremely efficient sorbents is needed. Among numerous ligands used in the liquid−liquid extraction (LLE) process, the diglycolamide-based (DGA) ligands play a leading role. Although these ligands display notable extraction performance in the liquid phase, their extractive chemistry is not widely studied when such ligands are tethered to a solid support. A detailed understanding of the relationship between chemical structure and function (i.e., extraction selectivity) at the molecular level is still missing although it is a key factor for the development of advanced sorbents with tailored selectivity. Herein, a series of functionalized mesoporous silica (KIT-6) solid phases were investigated as sorbents for the selective extraction of REEs. To better understand the extraction behavior of these sorbents, different spectroscopic techniques (solid-state NMR, X-ray photoelectron spectroscopy, XPS, and Fourier transform infrared spectroscopy, FT-IR) were implemented. The obtained spectroscopic results provide useful insights into the chemical environment and reactivity of the chelating ligand anchored on the KIT-6 support. Furthermore, it can be suggested that depending on the extracted metal and/or structure of the ligand and its attachment to KIT-6, different functional groups (i.e., C═O, N−H, or silanols) act as the main adsorption centers and preferentially capture targeted elements, which in turn may be associated with the different selectivity of the synthesized sorbents. Thus, by determining how metals interact with different supports, we aim to better understand the solid-phase extraction process of hybrid (organo)silica sorbents and design better extraction materials.

KEYWORDS: *solid-phase extraction, mesoporous silica, sorbents, rare earth elements, dynamic extraction, lanthanides*

1. INTRODUCTION

The term "rare earth elements" (REEs) is used to describe elements in the f-block of the periodic table—lanthanides (Ln) and includes scandium and yttrium. Except for the radioactive promethium, they are more abundant in the Earth's crust than platinum, gold, and silver.[1] Currently, the largest global producer of REEs is China, which possesses about 90% of the global REE supply, yet the Chinese government has recently cut down the production and export of REEs.[2,3]

Received: September 14, 2020
Accepted: November 17, 2020
Published: December 10, 2020

However, the consumption rate of REEs has been rapidly increasing over the last decade, and currently the demand for REEs is rising at a rate of about 5% yearly.[4,5] The importance of advanced and environmentally friendly technologies combined with a difficult geopolitical situation increases the need for pure REEs and their compounds. Depending on the targeted application, different purities and amounts of REEs are needed.[3,6] For instance, wind turbines necessitate approximately 600 kg of REEs per turbine, whereas much smaller quantities are required in batteries and phosphors lighting bulbs.[3,6] The need for large quantities of pure REEs is exacerbated by the fact that REEs are extremely difficult to separate due to their very similar physicochemical properties (i.e., valence state, size).[6] Moreover, the environmental impacts resulting from current REE purification/separation strategies, such as the production of unwanted wastes, the release of spent organic solvents, or the high water consumption need, have limited the widespread mining of REEs.[3,7,8] In fact, the largest reserves of REEs are in North America, Australia, and Brazil. However, due to stringent environmental regulations, mining activities in these regions are limited. Therefore, REE recycling/recovery strategies from alternative sources, such as red mud (residue from bauxite mining) or phosphogypsum (residue from phosphate rock mining), are critically and urgently needed.[3,9] Both sources have much higher levels of REEs compared to their original deposits because of the treatment on the mineral.[3,9] Economically relevant levels of REEs are also present in electronic wastes (e-wastes), such as hard drives, fluorescent lights, and permanent magnets or batteries.[3,10] Unfortunately, recovery and recycling of REEs and their compounds from e-wastes are still in the infancy, with only approximately 1% of REEs being reused.[3,11]

At the industrial scale, purification of REEs is based mostly on liquid−liquid extraction methods (LLE), but these purification procedures have a significant negative impact on the environment.[12] More environmentally benign methods, based on solid−liquid extraction (SLE) systems that use various resins, could minimize some of the adverse environmental impacts of LLE. Regrettably, ion-exchange materials often possess selectivity and preconcentration abilities too low to properly perform the required elemental separation. On the other hand, commercial extraction chromatographic resins based on impregnation often show insufficient reusability properties.[13,14] Fortunately, the recent development of functionalized nanomaterials designed to selectively extract or preconcentrate elements can provide a viable alternative to current methodologies.[15−18] In contrast to bulk sorbents, nanosorbents possess higher specific surface areas; hence, they may provide a higher accessibility to more extraction centers and consequently better extraction efficiency.[9,15−19] Moreover, the chemical tethering of the functional groups or chelating/complexing ligands on the silica surface through silane coupling methods provides sorbents with a substantially higher chemical stability, resulting in a higher potential for reuse.

Over the last decade, much effort has been devoted to the development of efficient and highly selective ligands for LLE processes.[18,20−24] From this research has emerged a family of particularly interesting molecules, the diglycolamide-type (DGA) ligands, which can be easily synthesized and are known as effective extractants of trivalent f-elements with a lower affinity toward transition metals or actinides.[15,20−22,25−27] Most of the studies indicate that lanthanide ions form 1:3-type complexes with DGA-based ligands (Ln^{3+}/DGA = 1:3) in a dissolved environment where the DGA-type ligand exhibits a stepwise complexation with the metal center.[20,25,26] In contrast, actinides such as UO_2^{2+} and NpO^{2+} ions exist mostly as 1:1 and 1:2 complexes, respectively.[25] Metal ions with coordination number 9 are bonded to the DGA-type ligands via three oxygen atoms, i.e., through two carbonyl groups (C═O) and one C−O−C donor group. Some recent studies have highlighted that although lanthanides display a pronounced preference toward higher coordination numbers, the geometry can be fine-tuned by modifying the ligand and the coordination environment.[28] Particularly, the chelating angle (or "bite-angle") of the extractant, i.e., the angle between three oxygen atoms, plays a crucial role in the coordination and thus, in the selectivity of the diglycolamide-based ligands.[15] Nevertheless, it should be kept in mind that chemical properties of lanthanides and ligand affinity for all REEs are usually very similar and, in the end, mostly the ionic radii (i.e., La^{3+} (103 pm) > Nd^{3+} (98.3 pm) > Eu^{3+} (94.7 pm) > Dy^{3+} (94.2 pm) > Er^{3+} (89 pm))[29] drive the interactions between metal ions and ligands. It is important to note that tethering of the ligand on a solid surface rigidifies the chemical structure of the complexant, thus enhancing the importance of the chelating angle, as recently demonstrated.[9,15,17,30] Despite a large number of studies dealing with metal separation/extraction processes, this aspect is still scarcely presented, studied, and understood from a fundamental perspective.

Spectroscopic methods, i.e., X-ray photoelectron spectroscopy (XPS), Fourier transform infrared spectroscopy (FT-IR), and solid-state nuclear magnetic resonance (NMR) analyses, are powerful techniques that offer structural insights at the atomic level.[31−37] Although many studies have been reported on different silicas and different grafted ligands,[9,15,24,37−39] questions related to the binding interactions between sorbents and REEs, the exact origin of REE selectivity, and the mechanisms involved, are still not entirely answered. The nature of the hydroxyl groups (e.g., isolated, hydrogen-bonded) and ligand moieties, their amount, density, and distribution (e.g., uniformly or randomly dispersed), are the main factors that can alter the selectivity of sorbents. Moreover, attachment of the ligand on a solid surface narrows and rigidifies the chelating ligand binding angle, thus reducing the mobility of the ligand and consequently improving the selectivity of such a system toward specific elements, as compared to the extraction in the liquid phase with the same ligand.[15]

To complement our past studies, where we focused on the extraction performance of silica-based hybrid nanosorbents, this work concentrates on deciphering the role of the functional groups that are enhancing the interaction and selectivity of the modified silica sorbents with rare earth elements.[9,15,16,40] In-depth knowledge of the bonding interactions between the sorbents and metals is required since our current understanding of the selectivity and of the adsorption mechanisms remains quite rudimentary. For that purpose, a number of tailor-made nanoporous silica sorbents functionalized with various chelating ligands, such as diglycol-2,4-diamido-propyltriethoxysilane (DGA-N), 3,6-dioxaoctanediamido-propyltriethoxysilane (DOODA-N), and furan-2,4-diamido-propyltriethoxysilane (FDGA-N), were selected. The choice of KIT-6 as a support material to form solid-phase extraction (SPE) sorbents was based on its highly inter-

https://dx.doi.org/10.1021/acsami.0c16282
ACS Appl. Mater. Interfaces 2020, 12, 57003−57016

connected three-dimensional (3D) cubic pore network, which was shown to be more favorable for the transport of liquid phases through the pores and have higher resistance to pore-blocking phenomena.[41] The SPE sorbents were compared both in a batch extraction mode and in a flow-through column system, and significant differences were observed in these conditions, which could be correlated to the nature of the surface coordination environment involved.

2. EXPERIMENTAL DETAILS

2.1. Material Synthesis and Functionalization. The support material, KIT-6 silica powder, was obtained following the procedure reported by Kleitz et al.[42] Briefly, 9.0 g of Pluronic P123 ($EO_{20}PO_{70}EO_{20}$, Sigma-Aldrich) was dissolved in distilled water (325.0 g) and 17.4 g of HCl (37%) was added under vigorous stirring. After complete dissolution, 9.0 g of *n*-butanol (BuOH, Aldrich, 99%) was added. The reaction mixture was left under stirring at 35 °C for 1 h, after which 19.4 g of tetraethoxysilane (TEOS, Sigma-Aldrich, 99%) was added at once. The mixture was left under stirring at 35 °C for 24 h, followed by an aging step at 100 °C for 24 h under static conditions. The resulting solid product was filtered and dried for 24 h at 100 °C. Extraction in an ethanol−HCl mixture was used for template removal, followed by calcination in air at 550 °C. The syntheses of the ligands (DGA-N, FDGA-N, and DOODA-N) and their silanization were performed as previously reported.[15,16] Details of the ligand synthesis are given in the Supporting Information. Ligand grafting was also performed according to the literature,[15,16] except for the grafting of the DOODA ligand that was done either in reflux conditions (120 °C) for 24 h (material labeled as KIT-6-N-DOODA-120) or at room temperature for 48 h (material labeled as KIT-6-N-DOODA). Also, compared to a previous report,[15] where 300 mg of FGDA-APTS ligand was grafted on KIT-6 (noted as KIT-6-N-FDGA), we also grafted a higher concentration of ligand, i.e., 600 mg. This material was labeled as KIT-6-N-FDGA-600.

2.2. Metal-Loaded Sorbents. Prior to the extraction experiments with Ln^{3+}, pure KIT-6 material and the hybrid sorbents were thermally pretreated to remove physisorbed water. The silica material (KIT-6) and DGA-N-, FDGA-N-, or DOODA-N-modified sorbents (200 mg) were soaked overnight in saturated solutions of selected elements prepared from nitrate salts (i.e., $Nd(NO_3)_3$, $Gd(NO_3)_3$, $Eu(NO_3)_3$, $Sc(NO_3)_3$) or $Fe(NO_3)_3$ at room temperature. After this loading step, metal-containing materials were filtered and dried at 40 °C for 48 h. The resulting products were labeled as KIT-6-N-DGA-X, KIT-6-N-DOODA-X, or KIT-6-N-FDGA-X, respectively, where X corresponds to the metal ion that was loaded (i.e., Nd^{3+}, Eu^{3+}, Sc^{3+}, Gd^{3+}, Fe^{3+}). The various REEs used here in our spectroscopic investigations were selected based on their preferential extraction uptake, as established in our previous studies.[15,16] Moreover, this selection of elements allows us to examine the relation between the metal cations and the cavity size of the chelating ligand to better investigate the metal complexation mechanism and the ligands' selectivity. To compare the extraction behavior between REEs and most common competing elements, which also exist as trivalent ions, materials were also similarly saturated with iron salt. The saturated materials were subjected to Fourier transform infrared spectroscopy (FT-IR), XPS, and solid-state NMR analysis.

2.3. Characterization Techniques. Low-temperature (−196 °C) nitrogen physisorption isotherms were measured using an Autosorb-iQ2 from Quantachrome Instruments (Anton Paar, Boynton Beach, FL). The pore size distributions were calculated by applying the silica NLDFT model, considering an amorphous SiO_2 surface and a cylindrical pore model, taking into account the desorption branch.[43] Prior to the analysis, samples were outgassed at 200 °C (unmodified silica support) or at 80 °C (functionalized sorbents). The specific surface area (S_{BET}) was determined, in the range P/P_0 = 0.05−0.2, using the Brunauer−Emmett−Teller equation, and the total pore volume (V_{pore}) was measured at P/P_0 = 0.95.

A Bruker Avance NEO 500 wide-bore system (Bruker BioSpin, Rheinstetten, Germany) was used to obtain solid-state NMR spectra. For ^{13}C and ^{29}Si NMR, samples were packed inside a 4 mm rotor and measured on a triple resonance magic angle spinning (MAS) probe operating in a dual mode. The rotor spinning was set to 14 kHz (^{13}C) or 8 kHz (^{29}Si). The resonance frequencies for ^{13}C and ^{29}Si were 125.78 and 99.38 MHz, respectively. Cross-polarization (CP) was achieved by a ramped contact pulse from 50 to 100% with a contact time of 2 ms for ^{13}C and 5 ms for ^{29}Si. During acquisition, ^{1}H was high-power-decoupled using SPINAL with 64 phase permutations. ^{29}Si was measured without cross-polarization using a relaxation delay of 60 s. The chemical shifts are reported in ppm and are referenced externally to adamantane for ^{13}C by setting the low field signal to 38.48 ppm and to 4,4-dimethyl-4-silapentane-1-sulfonic acid (δ = 0 ppm) for ^{29}Si. ^{1}H NMR spectra were acquired with a single pulse experiment on a 2.5 mm $^{1}H/^{19}F$-X probe at a resonance frequency of 500.22 MHz and a rotor spinning speed of 30 kHz. As external reference, DSS was used (δ = 0 ppm).

Coupled thermogravimetric analysis-differential thermal analysis (TGA-DTA) was performed using a Netzsch STA 449C thermogravimetric analyzer, under airflow (20 mL min^{-1}) with a temperature-programmed heating rate of 10 °C min^{-1}.

X-ray photoelectron spectroscopy (XPS) measurements were conducted on a Kratos (UK) AXIS-ULTRA instrument with a monochromatic Al X-ray source operated at 300 W. Silica-ligand-containing samples were measured in the powder form, whereas metal-loaded materials were analyzed as pellets. High-energy-resolution spectra were recorded at 20 or 40 eV pass energy and step size of 0.05 or 0.1 eV. The binding energy (BE) scale was calibrated against standard samples: Au $4f_{7/2}$: 83.950 eV; Ag $3d_{5/2}$: 368.2 eV; and Cu $2p_{3/2}$: 932.6 eV.

The FT-IR spectra were recorded on a Nicolet FT-IR spectrometer 5 SXC. The measurements were carried out with a resolution of 4 cm^{-1} and scan number of 64 time/sample in the 4000−400 cm^{-1} range. The powders were pressed into a thin self-supporting pellet and placed inside an IR cell equipped with KBr windows. All spectra were recorded after 2 h of outgassing pretreatment at RT using a vacuum frame (residual pressure < 10^{-3} mbar).

Transmission electron microscopy (TEM) was performed using a Philips G2 F30 Tecnai instrument operated at 300 kV. The powder samples were dispersed in acetone and sonicated (15 min) in a sonic bath. Then, 5 μL of the suspension was placed onto a carbon micro-grid and allowed to dry before measurements (KAIST, Daejeon, Republic of Korea).

Low-angle powder X-ray diffraction (XRD) patterns were recorded on a Rigaku Multiplex instrument operated at 2 kW, using Cu Kα radiation (KAIST, Daejeon, Republic of Korea). The XRD scanning was performed under ambient conditions in steps of 0.01°, with an accumulation time of 0.5 s.

2.4. Extraction Procedures. The extraction performances of the hybrid silica sorbents (i.e., KIT-6-N-DGA, KIT-6-N-FDGA, KIT-6-N-DOODA) were investigated for the mixture of REEs or REEs with additional elements either in a batch or in a flow-through (column) mode. In the case of the batch extraction mode, the solution/solid ratio was fixed at 500 (V/m). The initial and final concentrations of metals in nitric acid solutions (pH 4) were determined by inductively coupled plasma mass spectrometry, ICP-MS (model 8800, Agilent Technologies), and used to calculate the extraction capacity (E, %), distribution constant (K_d, mL g^{-1}), and breakthrough volumes ($V_{b,\%}$, mL) for all the materials tested. Solutions of analytes and internal standard were prepared from commercial solutions (Plasma, Cal, SCP Science). Next, 10 mg of nanosorbent was stirred for 30 min with the mixture of analytes (15 μg L^{-1}), and then, the supernatant was subsequently filtered through a 0.2 μm syringe filter and analyzed by ICP-MS. Kinetics and isotherm studies were performed in the batch extraction mode with the contact time varying from 1 to 60 min, for kinetics investigation, and the concentration of REEs ranging from 5 up to 300 μg L^{-1}, for isotherm studies. All experiments were performed in triplicates, and only the average values are provided. In the case of dynamic (flow-through) extraction studies, 150 mg of

https://dx.doi.org/10.1021/acsami.0c16282
ACS Appl. Mater. Interfaces 2020, 12, 57003−57016

Scheme 1. Schematic Representation of the Synthesis of Different DGA-Based Silanes (a) and Example of the Grafting Procedure (b)

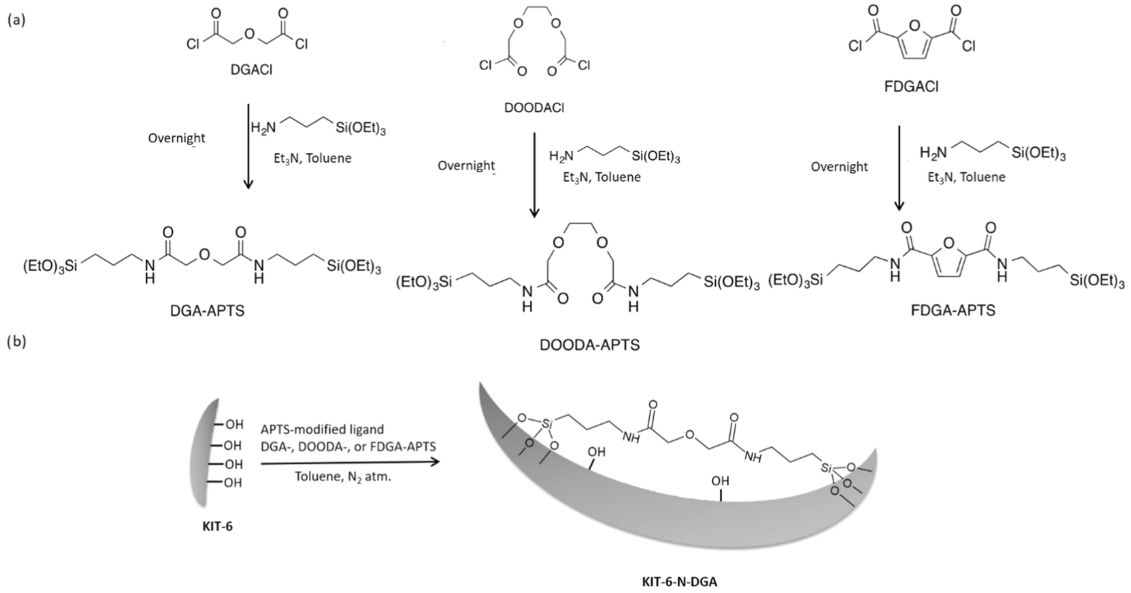

commercial DGA resin and either 30 or 100 mg of mesoporous sorbents were packed inside 2 mL SPE cartridges through a slurry-packing method. Filled cartridges were washed with high-purity water and conditioned with pH 4 HNO_3. Then, a solution of europium or an REE mixture (10 mg L^{-1} per element) was loaded onto the column, with the flow rate of 1 mL min^{-1}.

3. RESULTS AND DISCUSSION

3.1. Structural and Textural Characterization of the (Organo)silica Sorbents. To determine the influence of the nature of the ligand (i.e., its structure, composition, or its grafting procedure) on the extraction performance, different DGA-based derivatives were chemically anchored on mesoporous KIT-6 silica support (Scheme 1). Grafting these ligands allowed us to finely tune the sorbent chelating angle and thus obtain materials with selectivity toward various groups of metals (Figure 1).[15] Typically, mid-size elements were

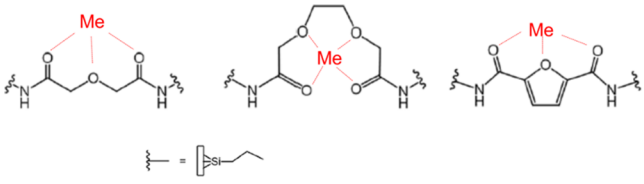

Figure 1. Different coordination angles (i.e., "bite angles") of various mesoporous silica-grafted DGA-type ligands.

preferentially extracted by the KIT-6-N-DGA sorbent, while the material modified with ligands with smaller chelating angles, e.g., KIT-6-N-DOODA, exhibited higher extraction capacities toward smaller (heavier) lanthanides. On the other hand, the material functionalized with the furan-based ligand, e.g., the KIT-6-N-FDGA sample, did not demonstrate interesting selectivity within lanthanides, yet its selectivity toward Sc was significant.[15] The synthesis and modification conditions of the mesoporous sorbents were selected carefully to obtain materials either with an equivalent amount of ligand or with comparable porosity characteristics, as listed in Table S1 and Figure S1. In comparison to pure KIT-6 silica (specific surface area: 910 m^2 g^{-1}; mode pore size: 8.1 nm; and pore volume: 1.21 cm^3 g^{-1}), all adsorbents showed reduced pore sizes (reduction from 8.1 to 7.6−7.3 nm), total pore volume (drop from 1.21 to 0.78 cm^3 g^{-1}), and specific surface area (decreased to about 500−600 m^2 g^{-1}).[15,16] Significantly lower specific surface area (S_{BET} = 376 m^2 g^{-1}) and pore size (7.1 nm) were observed for materials modified with 600 mg of the FDGA ligand. Therefore, a second grafting using a substantially reduced (300 mg) amount of this ligand was attempted, leading to a sorbent-specific surface of about 500 m^2 g^{-1} area and pore size around 7.3 nm, and the material was labeled KIT-6-N-FDGA (Figure S1 and Table S1). After ligand-anchoring, the original microporosity of the KIT-6 material (0.06 cm^3 g^{-1}) is no longer present, no matter which ligand was grafted on the surface. Furthermore, the 3D pore organization of the functionalized KIT-6 sorbents was verified by low-angle powder X-ray diffraction (XRD) and transmission electron microscopy (TEM) (Figure 2). The TEM images reveal that the highly ordered cubic pore structure survives well the grafting conditions and remains stable after ligand-anchoring. The low-angle XRD patterns of all mesoporous sorbents (Figure 2d) display diffraction peaks, which could be indexed to the 3D cubic $Ia3d$ symmetry.[42,44] A unit cell size of 24.3 nm was calculated from the XRD data ((211) peak of the cubic $Ia3d$ phase) for the pure KIT-6 material. The ligand-grafted materials displayed an evident shift in the 211 reflection toward higher 2Θ values and had consequently lower unit cell sizes, i.e., 23.3 nm (KIT-6-N-DGA), 22.8 nm (KIT-6-N-FDGA), and 22.3 nm (KIT-6-N-DOODA), implying either a possible shrinkage of the mesostructure upon the reflux/grafting procedure and/or higher framework condensation during this procedure.

3.2. Mesopore Surface Characterization. The structure and composition of the resulting mesoporous hybrid sorbents were further studied by thermal analysis (Table S1 and Figure S2), solid-state NMR (Figure 3), Fourier transform infrared spectroscopy (Figure 4), and X-ray photoelectron spectroscopy (Figure 5 and Table S2). The total weight change indicated via thermogravimetric analysis shows above 20% mass loss for

https://dx.doi.org/10.1021/acsami.0c16282
ACS Appl. Mater. Interfaces 2020, 12, 57003−57016

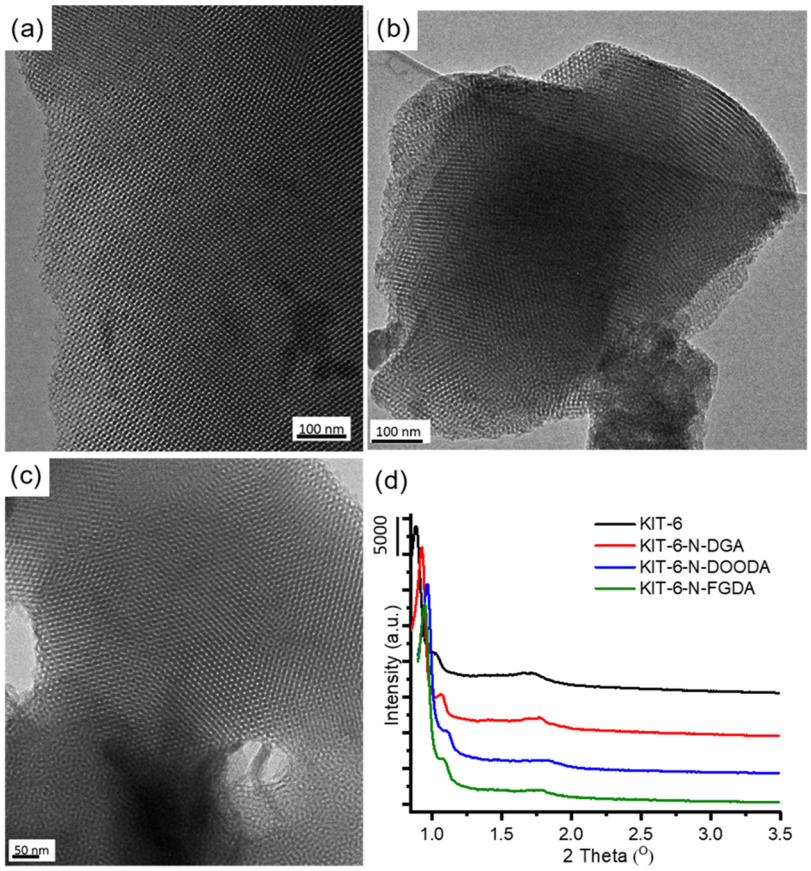

Figure 2. Representative TEM images (a–c) and low-angle XRD patterns (d) of the obtained nanoporous hybrid sorbents: (a) KIT-6-N-DGA; (b) KIT-6-N-DOODA; (c) KIT-6-N-FDGA; and (d) XRD plots of the materials, as indicated.

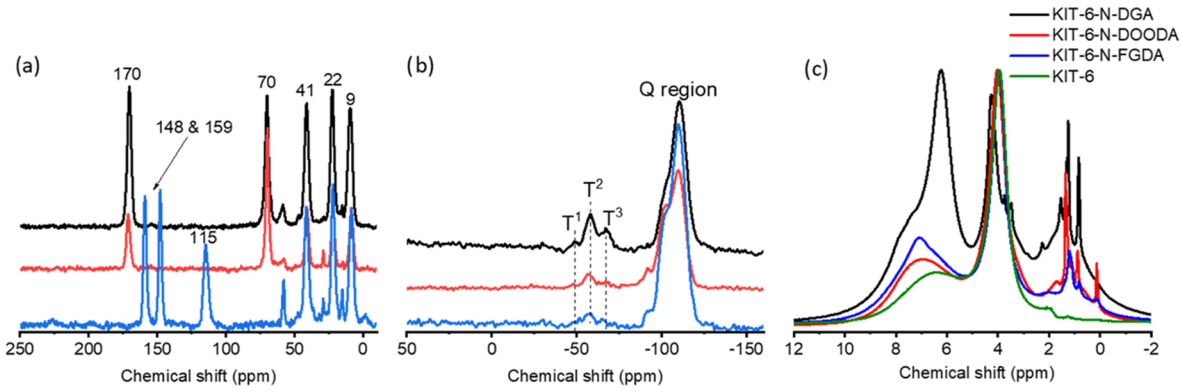

Figure 3. Solid-state NMR spectra of all of the materials: (a) ^{13}C CP NMR, (b) ^{29}Si MAS NMR, and (c) ^{1}H MAS NMR.

all the synthesized materials, except for the KIT-6-N-FDGA material, which shows only 15% mass loss (Table S1 and Figure S2). The thermal decomposition of all hybrid materials occurred in the temperature range between 150 and 650 °C, and besides KIT-6-N-DOODA-120, all sorbents showed one broad exothermic effect between 320 and 370 °C, attributed to the decomposition of the DGA-type ligand. The presence of two decomposition peaks at 276 and 330 °C, in the case of the KIT-6-N-DOODA-120 material grafted in typical grafting conditions (i.e., at 120 °C overnight), may suggest a partial cleavage of the ligand or attachment through only one side of the silane upon modification (see Scheme 1). Therefore, grafting of this ligand was also performed at room temperature for 48 h; the resulting material is noted to be KIT-6-N-DOODA. Clearly, for this sample, a single decomposition peak was observed (Figure S2). Further, on comparing two sorbents modified with different amounts of the FDGA ligand, KIT-6-N-FGDA and KIT-6-N-FDGA-600, a slight shift to lower decomposition temperatures can be observed for the material with a lower amount of the ligand. This temperature shift may indicate an enhanced diffusion of oxygen inside the material or a better flow of the decomposition products out of the pores, which may further suggest a variation in the mass transport properties of this material, which will be essential for an enhanced transit of liquids.[41] The chemical environment of the attached ligands was further probed by solid-state ^{13}C CP, ^{29}Si MAS, and ^{1}H MAS NMR analyses (Figure 3). The results from ^{13}C CP and ^{29}Si MAS NMR analyses are in agreement with

https://dx.doi.org/10.1021/acsami.0c16282
ACS Appl. Mater. Interfaces 2020, 12, 57003−57016

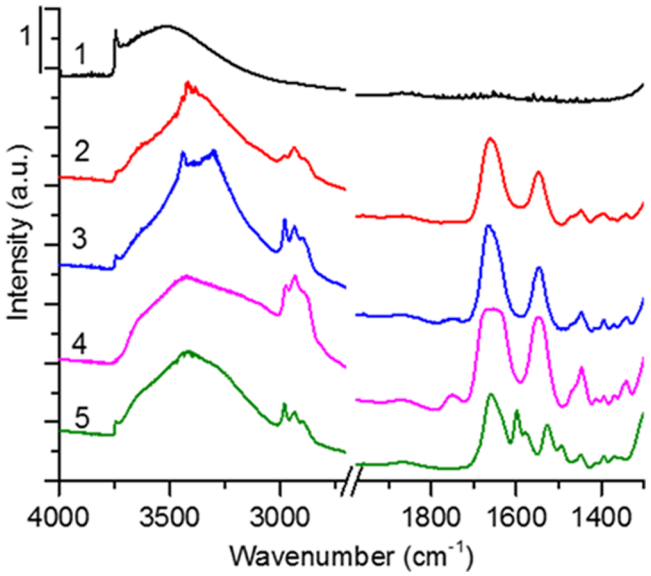

Figure 4. FT-IR absorbance spectra for the pristine silica material and modified samples, after outgassing at room temperature in vacuum for 2 h: (1) KIT-6, (2) KIT-6-N-DGA, (3) KIT-6-N-DOODA, (4) KIT-6-N-DOODA-120, and (5) KIT-6-N-FDGA.

previous reports, for both the position and intensity of the NMR signals.[15] In detail, the occurrence of peaks at about 9, 22, and 41 ppm confirms the successful grafting of the aminopropyltriethoxysilane.[15] The peak at about 170 ppm validates the presence of the C═O of the amide group, and the peak at about 70 ppm confirms the occurrence of the CH_2 group linked to the ether oxygen, for both KIT-6-N-DGA and KIT-6-N-DOODA hybrid materials.[15,45,46] In comparison, the position of the amide band (C═O) is shifted to lower values, i.e., 159 ppm, for the KIT-6-N-FDGA sample. The presence of the furan ring was further validated by the appearance of two consecutive bands at about 115 and 148 ppm.[15] The carbon peaks at 23 and 60 ppm that can be allocated to the carbon atoms in remaining ethoxy groups ($-Si-O-CH_2-CH_3$ moieties)[47] are visible for the KIT-6-N-FDGA sorbent, while the intensity of these peaks is much lower for the other two materials. None of the ^{13}C CP NMR spectra revealed the presence of the C═O bond for COOH groups or signals assigned to the "free" propyl chain (unmodified) in the amino groups.[45,46,48] This observation confirms that cleavage of the ligand did not occur during the modification step and ligands are grafted from both sides to the silica surface (see Scheme 1). The formation of T sites (T^3: $((SiO)_3Si-R)$; T^2: $((SiO)_2(OR)-Si-R)$; T^1: $((SiO)(OR)_2Si-R)$) for all modified silicas indicates that functionalization of the KIT-6 surface was effective and the chelating ligands were covalently attached to the surface.[37,49] The synthesized sorbents exhibited a mixture of various T^1-T^3 species with the dominance of T^2 sites (Figure 3b).

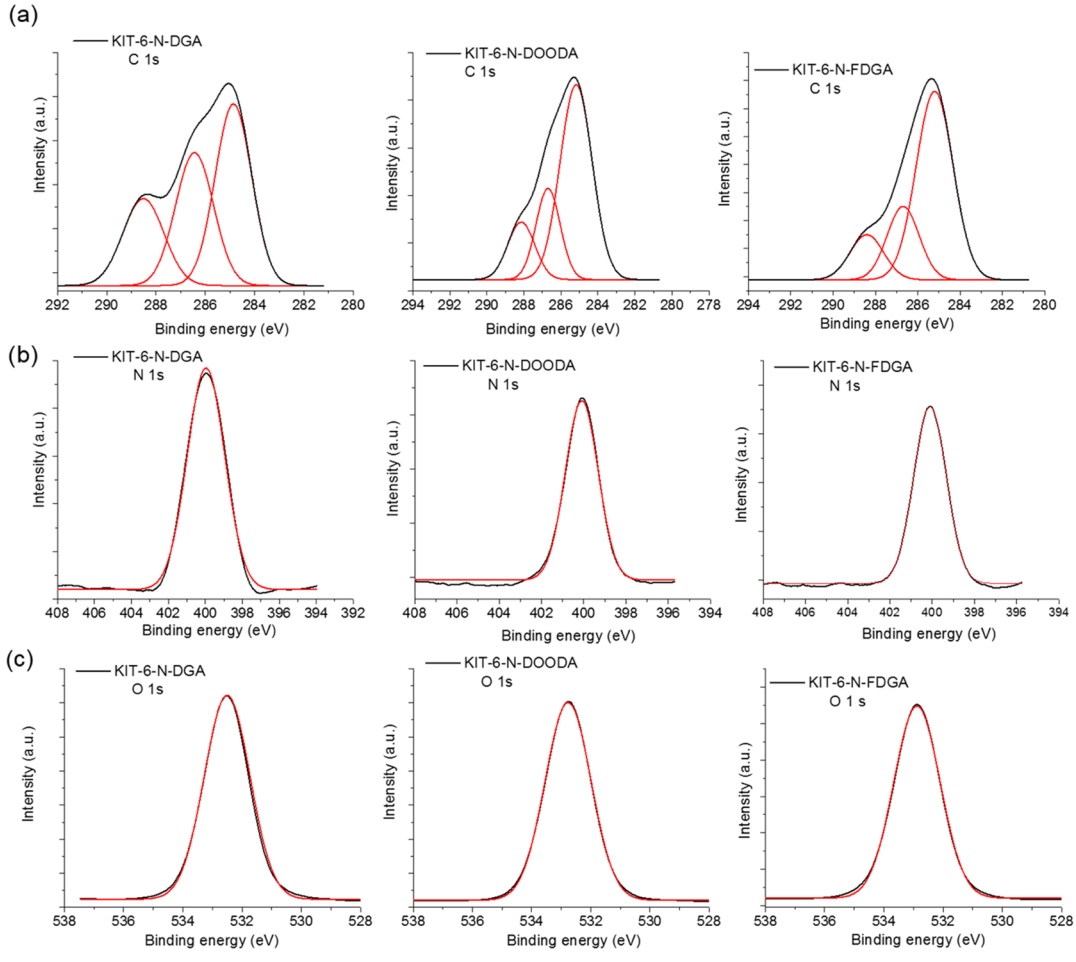

Figure 5. XPS spectra of KIT-6-N-DGA, KIT-6-N-DOODA, and KIT-6-N-FDGA materials for carbon (a), nitrogen (b), and oxygen (c).

https://dx.doi.org/10.1021/acsami.0c16282
ACS Appl. Mater. Interfaces 2020, 12, 57003−57016

The surface reactivity (i.e., extraction capacity) of a silica support not only is determined by the amount and accessibility of the grafted functional groups but also depends on the amount of the residual surface hydroxyl groups and their chemical/structural environment.[31] It was shown that surface silanols can act as synergistic reactive sites in metal-ion extraction; thus, their number and distribution are crucial factors.[50,51] The surface of amorphous silica reveals a variety of sites, for instance, isolated, vicinal, and geminal silanols, hydrogen-bonded silanols, or hydrogen-bonded water clusters. The number of sites depends on the origin of the silica, the synthesis, the thermal treatments, the modification procedures applied, or even on the storage conditions.[31,37] However, details related to the character of the surface silanol groups (isolated or fully/partially hydrogen-bonded) and their distribution (uniform or random distribution) are still missing, and the assignment of the different peaks, especially in the ^{1}H NMR spectra, often remains uncertain.[31−34] In our case, the presence of adsorbed water molecules on the surface of the pure KIT-6 material can be confirmed by the existence of an intense peak at 3.95 ppm in the ^{1}H NMR spectrum (Figure 3c).[31] In addition, the appearance of peaks of low intensity in the 1.8−2.1 ppm region indicates the existence of a small fraction of non-hydrogen-bonded (isolated), single, and/or geminal silanols.[31] The wide resonance band situated between 5.5 and 8 ppm, and centered at around 6.5 ppm, can be assigned to the silanol (SiOH) protons that are firmly H-bonded to the silica framework.[31] In contrast to non-functionalized KIT-6 silica, the grafted samples show the existence of well-resolved signals at a high resonance field, i.e., 0.15−1.7 ppm, which can be assigned to the alkyl (i.e., CH_2) protons, clearly indicating a successful grafting, with some remaining ethoxy groups (CH_3-CH_2-O-).

Furthermore, the results from ^{29}Si solid-state MAS NMR analysis enabled us to estimate the total amount of silanols (SiOH) and the Q^n silicon ratios (see Table S3).[37] Based on Q^n species calculations, the pure KIT-6 material possesses approximately 80 and 20% of single and geminal silanols, respectively, which is comparable with the literature data for SBA-15 silica (88% single and 12% geminal silanol groups).[37] After ligand-anchoring, the amount of single SiOH groups appears to have increased, while the number of geminal silanols significantly decreased, i.e., from 20% for pure silica to 3 and 7% for KIT-6-N-DOODA and KIT-6-N-FDGA materials, respectively. The Q^n calculations also show that the total amount of silanol groups is different for various sorbents, and the highest number of residual silanols was observed for DOODA- and FDGA-modified materials compared to the DGA-functionalized sorbent.

In agreement with the NMR results, FT-IR analysis also confirmed the existence of an amide band, i.e., the presence of a C═O stretching band (amide I) in the 1660−1680 cm^{-1} region and an amide II band at about 1550 cm^{-1} (NH deformation, CN stretching) (Figure 4).[52] The peaks observed in the 3000−2870 cm^{-1} region, assigned to C−H stretching, are visible for all of the modified materials.[53] Additionally, KIT-6-N-FDGA clearly shows the characteristic bands of 2,5 disubstituted furans, i.e., bands related to C═C stretching and ring-stretching vibration at about 1640 (shoulder), 1600, and 1525 cm^{-1}.[1,54] Visibly, after ligand-anchoring (Figure 4), the band assigned to the free (isolated) silanols (~3740 cm^{-1})[37] is reduced, as compared to pure KIT-6. Additionally, the FT-IR analysis confirms that the conditions typically used in this work (overnight grafting in dry toluene at 120 °C) caused a cleavage of the DOODA ligand and/or only its partial grafting. Indeed, two distinct C═O bands can clearly be observed for the KIT-6-N-DOODA-120 material (Figure 4), i.e., bands at 1660 and 1750 cm^{-1}, the latter band being indicative of the presence of COOH groups.[46,49,52] Oppositely, the grafting performed at room temperature for an extended period of time (48 h) leads to the preservation of the ligand chemical structure. Based on these observations, the rest of the investigation was performed with the KIT-6-N-DOODA sorbent obtained with a grafting at room temperature.

Moreover, the XPS results for C, N, and O also confirm that the grafting procedures were essentially successful (Figure 5 and Table S2). The presence of the DGA-type ligands was validated by the occurrence of carbon signals around 285 eV attributed to C−C/C−H bonds in the aliphatic chains, above 286 eV ascribed to C−O/C−N bonds, and another one above 288 eV associated with O-C-O/C═O (amide) species.[35,56] For all of the materials analyzed, the existence of C═O from COOH groups (peak above 290 eV) could be excluded.[57] For nitrogen and oxygen atoms, only one peak was observed at ~400 eV (N−C═O) and 532 eV, respectively. The O 1s spectrum showed the primary peak at a binding energy (BE) of ~532 eV assigned to silica (−Si-O−Si). Unfortunately, the strong broad peak of silica oxygen results in a poor fitting of the lower BE peak at about 531 eV, which is due to the ligand functionalities, i.e., C═O, C−O, or O═C−N species.[35,36,56]

3.3. REE Extraction Behavior. The extraction properties of the synthesized nanoporous sorbents were previously evaluated in the batch extraction mode.[15] High affinity, in terms of high distribution coefficients (K_d; mL g^{-1}), and pronounced selectivity were observed for KIT-6-N-DOODA and KIT-6-N-DGA materials, as compared to pure silica (KIT-6) or a commercial DGA resin. Notably, the hybrid materials showed much lower selectivity toward competing elements, making the REE extraction procedure with these sorbents more interesting industrially and potentially more economical and effective. Taking into account the K_d values for the most extracted elements, the KIT-6-N-DGA and KIT-6-N-DOODA mesoporous sorbents showed an extraction efficiency that is twice that of commercial resins, i.e., $K_{d\,(Lu^{3+})}$ = 5503 mL g^{-1} (KIT-6-N-DOODA) and $K_{d\,(Gd^{3+})}$ = 4619 mL g^{-1} (KIT-6-N-DGA) vs $K_{d\,(Er^{3+})}$ = 2221 mL g^{-1} for the commercial product.[15] In contrast, the KIT-6-N-FDGA material demonstrated only moderate extraction capacity toward lanthanides (3+), but it revealed a very high uptake of scandium (3+).[15] The extraordinary uptake of Sc^{3+} may be associated with the preferential location of Sc^{3+} ions into the ligand cavity or with the higher density of accessible silanols on the surface of this material, which may contribute to Sc^{3+} uptake.[50] Indeed, spectroscopy analyses showed the lowest amount of grafted ligand and the highest amount of residual free silanols for the KIT-6-N-FDGA material.

Now, extraction kinetics were investigated (Figure 6a), and the data clearly show that equilibrium is reached within only a few minutes with the lanthanides (3+), which is much faster than for other investigated systems, including commercial resins.[16,19,30,58−60] On the other hand, the uptake of scandium (3+) significantly increases with the extraction time, and after 1 h, no residual scandium (3+) is present in the solution. To further characterize the adsorption process and high affinity of the KIT-6-N-FGDA material toward scandium ions, adsorption experiments were performed with an initial concentration

https://dx.doi.org/10.1021/acsami.0c16282
ACS Appl. Mater. Interfaces 2020, 12, 57003−57016

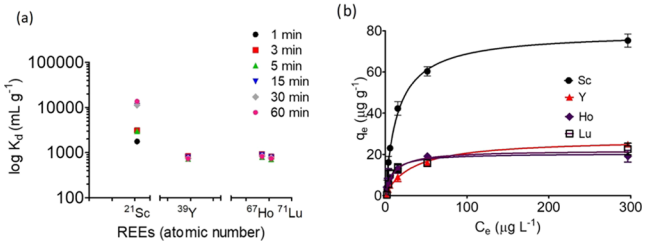

Figure 6. Effect of contact time on the REE uptake (a) and sorption isotherms (b) for selected elements and the corresponding Langmuir fitting model for the KIT-6-N-FDGA material.

of REEs ranging from 5 to 300 μg L^{-1}, and Langmuir and Freundlich adsorption models were used to fit the experimental data (Table S4). The Langmuir model is applicable to adsorption equilibrium systems where a monolayer adsorption with a defined number of equivalent adsorption sites exists and no interactions between adsorbates on neighboring sites occur. The empirical Freundlich model, on the other hand, is valid for heterogeneous adsorbent systems in a restricted range of adsorbate concentrations. Here, our results seem to fit better with the Langmuir model (Table S4), which is also in line with our previous studies,[9] suggesting rather homogeneous surface properties and a uniform monolayer adsorption process.

The extraction performance of the synthesized mesoporous sorbents was then studied in a flow-through (column) system, which allows us to estimate the working capacity of the sorbent, expressed as the breakthrough volume ($V_{b,\%}$)[41] (Figure 7). In our studies, the breakthrough volume represents

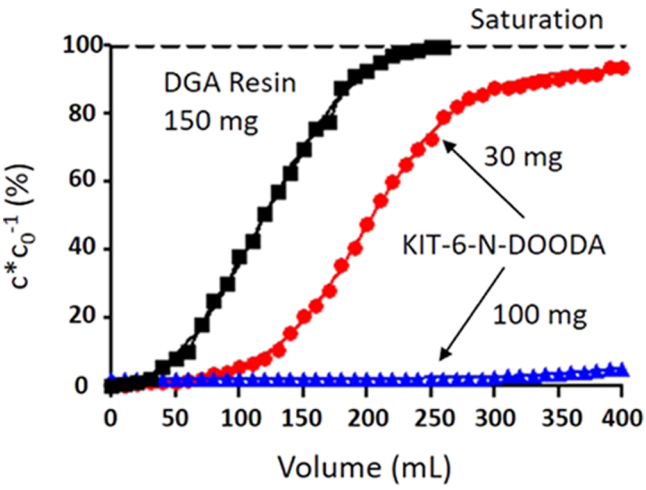

Figure 7. Comparison of the extraction behavior of the commercial DGA resin and the KIT-6-N-DOODA material in the dynamic extraction system.

the volume required to observe 5% elution of europium (3+) ions. Due to permeability issues of the KIT-6-based system,[41,51] we were not able to prepare columns with an equal amount of the mesoporous sorbent and of the commercial reference product. Therefore, dynamic studies were performed using 150 mg of the commercial DGA resin and 30 or 100 mg of KIT-6-based sorbents. Despite this limitation, the synthesized KIT-6-N-DOODA sorbent showed better extraction capacity than the commercial resin (Figure 7). In the case of the commercial DGA resin, 5% breakthrough volume was reached after flowing 40 mL of Eu^{3+} solution through the cartridge. On the other hand, 100 mg of the KIT-6-N-DOODA sorbent displayed significantly higher metal uptake, and 5% breakthrough volume was observed after passing almost 10 times higher volume of the Eu^{3+} solution (390 mL). Moreover, a cartridge made with only 30 mg of the hybrid silica powder still showed improved extraction capacity, and $V_{b,5\%}$ was recorded after loading approximately 100 mL of the Eu^{3+} solution. A similar behavior is also visible when the extraction procedure is performed with a mixture of lanthanides (Figure 8). Depending on the selected element, breakthrough volumes ($V_{b,10\%}$) 2−7-fold higher than those found for the commercial DGA resin were observed. These results clearly demonstrate the potential of the functionalized nanosorbents as solid-phase extraction materials. The silica SPE-type cartridges packed with higher amounts of mesoporous sorbents (i.e., above 100 mg) showed significant permeability/backpressure problems, indicating the necessity of utilizing specifically designed materials with hierarchical meso- and macropores,[51] which would greatly enhance transport of the liquid through the column.

The results from the dynamic studies, and particularly those related to the breakthrough volume values (Figure 8), in analogy to the data concerning the batch extraction experiments, show that the KIT-6-N-DOODA material has better extraction performance than KIT-6-N-FDGA. The batch experiments show no selectivity among Ln^{3+} for the KIT-6-N-FDGA material, while pronounced selectivity toward heavier elements was observed for KIT-6-N-DOODA. This translated into a K_d value for Lu^{3+} 3 times higher for KIT-6-N-DOODA than for KIT-6-N-FDGA. This proportion is somehow maintained in the dynamic experiment. In the dynamic studies, for heavier Ln, 10% elution of lutetium (3+) was observed after flushing the column with only 37 mL (KIT-6-N-FDGA) or ∼100 mL (KIT-6-N-DOODA) of the REE mixture solution (Figure S3). However, in the equilibrium conditions (batch), KIT-6-N-FDGA showed a much higher extraction capacity toward Sc^{3+} than the DOODA-modified sorbent, and such a trend was only slightly visible in the dynamic mode. Using the same materials, 10% elution of scandium (3+) was observed after passing through the column 30 mL (KIT-6-N-FDGA) or 50 mL (KIT-6-N-DOODA) of REE solution, respectively. One can hypothesize that Sc^{3+} retention on the KIT-6-N-FDGA material is mainly due to a limited number of covalent interactions with silanol (Si−O−Sc) and/or NH groups (see paragraph in Section 3.4) and that an exchange between the H^+ and Sc^{3+} ions, via the formation of covalent bonds between Sc^{3+} and the O- or N- moieties, is required for the extraction to occur.[38] It can be suggested that when the flow is rapid (i.e., dynamic experiments), the bond formation (Si−O−Sc) is too slow and only weak interactions can occur, leading to a lower retention. However, since Lu^{3+} ions interact mainly with the DGA-type ligand through multiple dative interactions, binding occurs rapidly and efficiently, leading to K_d values that are comparable between the dynamic and batch extractions.

3.4. Spectroscopic Surface Characterization of Metal-Loaded DGA-Silica Sorbents. The interactions between immobilized DGA, DOODA, or FDGA ligands and selected rare earth elements were further investigated by solid-state NMR (Figures 9 and S4), FT-IR (Figure 10), and XPS (Figures S5−S7 and Table S5) spectroscopies.

The adsorption of metal ions on the different silica-based sorbents causes changes on the proton NMR spectra (Figure

https://dx.doi.org/10.1021/acsami.0c16282
ACS Appl. Mater. Interfaces 2020, 12, 57003−57016

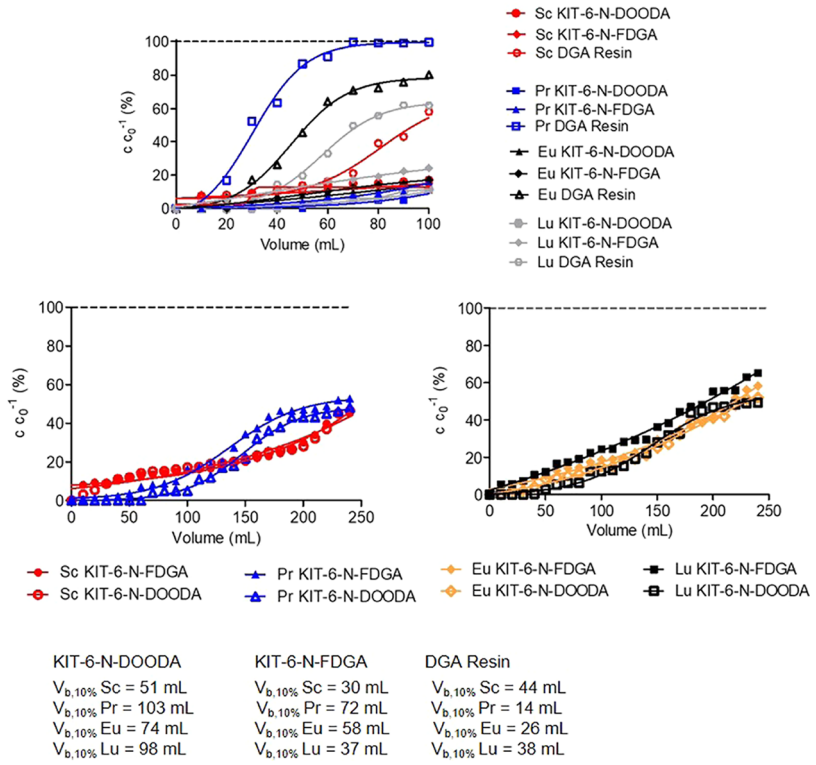

Figure 8. Comparison of the dynamic extraction capacities of the commercial resin and silica-based materials; for clarity, only selected elements are presented.

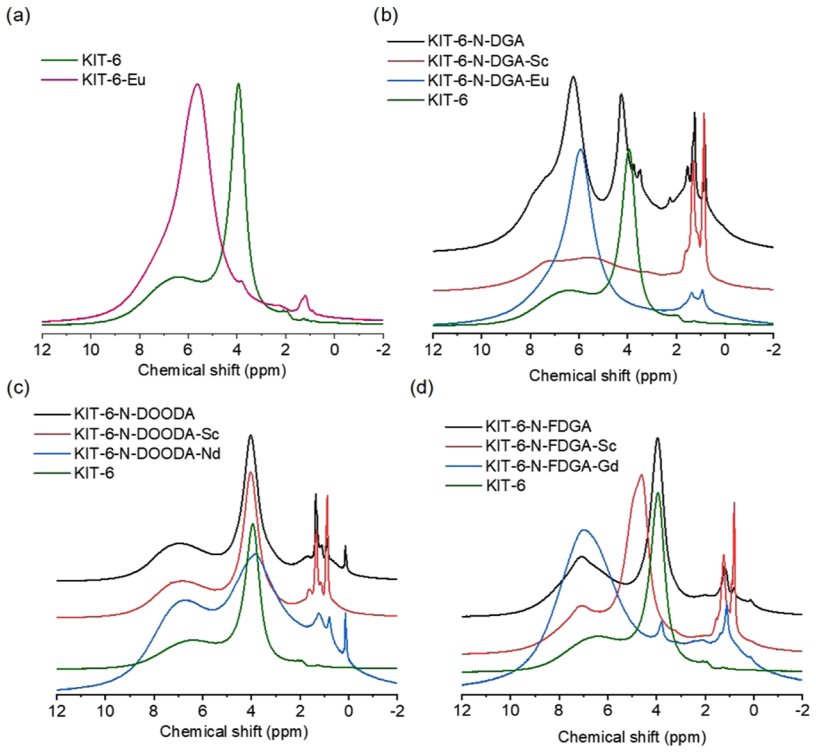

Figure 9. Solid-state ^{1}H NMR spectra of KIT-6 (a), KIT-6-N-DGA (b), KIT-6-N-DOODA (c), and KIT-6-N-FDGA (d) sorbents saturated with different metals, as indicated.

9). Depending on the element loaded and the type of ligand, different variations were observed. For instance, pure KIT-6 and KIT-6-N-DGA materials saturated with metals did not show the presence of adsorbed water molecules on their surface, as shown by the lack of the intense peak at ~4 ppm. Differently, KIT-6-N-DOODA and KIT-6-N-FDGA materials display only slight changes in that region upon metal loading. Note that the peak around 4 ppm can also be attributed to the

https://dx.doi.org/10.1021/acsami.0c16282
ACS Appl. Mater. Interfaces 2020, 12, 57003−57016

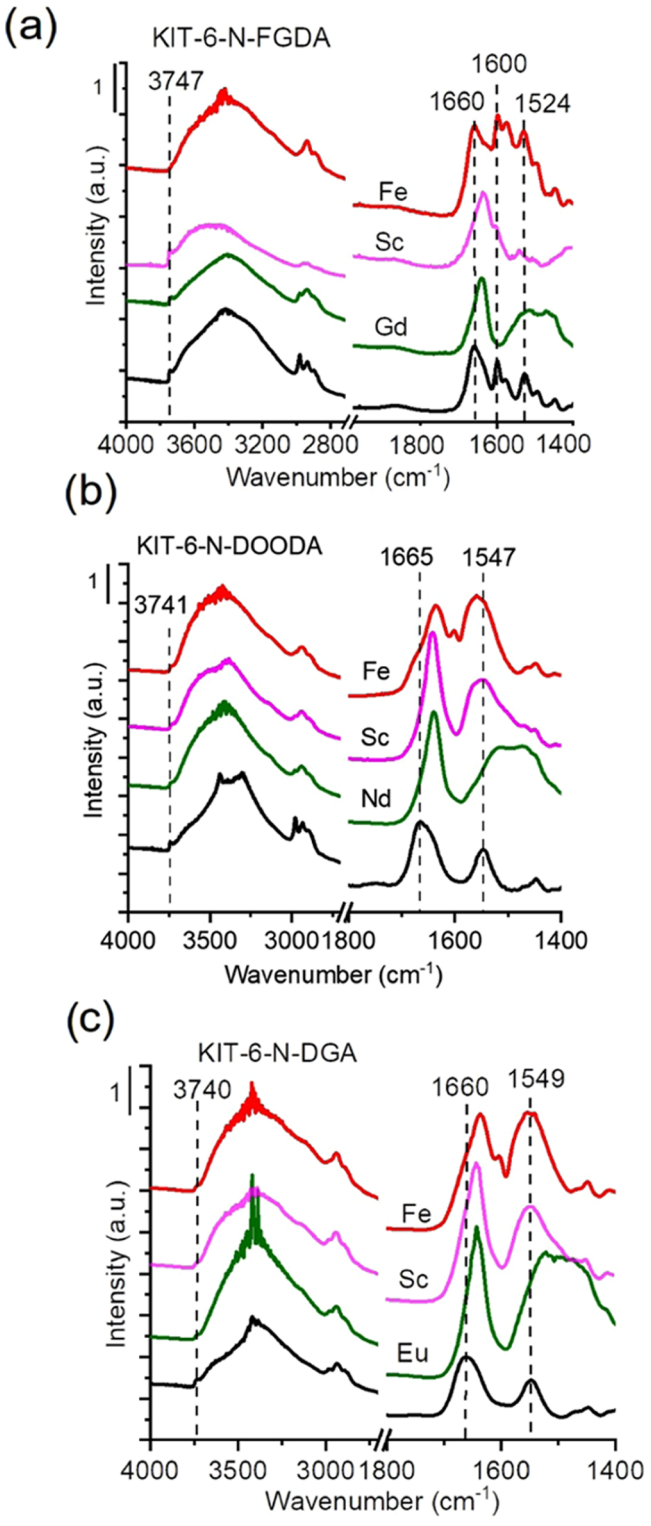

Figure 10. FT-IR absorbance spectra of KIT-6-N-FDGA (a), KIT-6-N-DOODA (b), and KIT-6-N-DGA (c) materials, before (black line) and after metal loading. Spectra were recorded after outgassing at RT in vacuum for 2 h.

water coordination sphere of metal ions.[38] Furthermore, significant variations were observed in the silanol region (6−8 ppm) due to the interaction of the hybrid surface with the metallic ions. In general, for all metal-loaded samples, the silanol-related peak is enhanced after lanthanide (3+) loading (Eu, Nd), while it declines after Sc^{3+} loading. Such a phenomenon may indicate that accessible/free silanols can act as specific binding sites for scandium ions upon loss of H^+.[38,50] In addition, metal-loaded samples show alteration in the peak intensity at a high resonance field, i.e., the 0.15−1.7 ppm region, which seems to be more prominent for Sc^{3+}-loaded materials than for lanthanide-loaded samples. This behavior may further implicate different binding sites for scandium than for Ln^{3+}(Figure 9).[61]

On the other hand, the ^{29}Si MAS NMR spectra (Figure S4) do not substantially change after introduction of different metal ions. It can be noticed that no significant change in intensity is observed after Sc^{3+} loading, while intensity variations are more pronounced when lanthanides (i.e., Eu^{3+}, Nd^{3+}) are added. In the case of the pure silica material, interactions with europium ions take place through the hydroxyl groups (e.g., Q^2 and Q^3 species), resulting in lower intensity of these peaks. This behavior suggests that metal ions can be strongly linked with the surface silanols. However, it should be kept in mind that the dia- or paramagnetic character of some of the rare earth ions could alter the NMR magnetic field, and therefore, these observations should be taken with caution.

Interactions between the grafted ligands and the metal ions are obvious based on the change in position and intensity for the various bands according to FT-IR spectroscopy (Figure 10). In general, the larger the shift and/or the intensity of the IR band upon metal adsorption, the higher is the affinity of the ligand toward the analyzed metals, i.e., stronger and more favorable are the ligand−metal interactions.[62,63] For KIT-6-N-FDGA, the FT-IR spectrum confirms the existence of the amide group, i.e., the band at about 1660 cm^{-1} (amide I band; C═O stretching), the band at 1577 cm^{-1} (amide II band; NH deformation, CN stretching), and bands related to C═C stretching and ring-stretching vibration at about 1640 (shoulder) and 1600 cm^{-1}, and 1525 cm^{-1}, respectively (Figure 10a).[52−55] After metal loading, all the samples show a lower intensity of the OH band (3740 cm^{-1}), as compared to the pristine sorbent. The Fe-containing sample does not show any shift of the amide I band (1660 cm^{-1}). On the contrary, upon the adsorption of Gd^{3+} and Sc^{3+}, the bands of the ligands appear at lower frequencies, overlapping with the ring vibration band at 1637 and 1633 cm^{-1} for KIT-6-N-FDGA-Gd and KIT-6-N-FDGA-Sc samples, respectively. In addition, a very tiny attenuation of the peak intensity after metal loading could also be observed. Similarly, upon rare earth metal loading (Sc^{3+} and Gd^{3+}), the amide II (1577 cm^{-1}) and ring-stretching vibration bands (1525 cm^{-1}) are combined together and shifted below 1525 cm^{-1} (Gd^{3+}) or around 1538 cm^{-1} (Sc^{3+}), whereas these bands are almost unperturbed after Fe^{3+} loading. Furthermore, the band at 1600 cm^{-1} is shifted after Gd^{3+} adsorption, while after Sc^{3+} loading, only the intensity diminishes. Once again, the KIT-6-N-FDGA-Fe material does not display any significant changes in this region. The distinct behavior of Fe^{3+}-FDGA and Ln^{3+}-FDGA complexes tethered on silica may indicate that the amide oxygen atom acts as a coordination site for REEs but not for Fe^{3+}.[63−65] The largest shift toward lower wavenumbers for the amide I band (from 1660 to 1633 cm^{-1}) was observed for Sc^{3+}-loaded materials, which may implicate a greater affinity toward Sc^{3+} than to other metals (e.g., Gd^{3+}, Fe^{3+}), for this sorbent. In a similar manner, the KIT-6-N-DOODA sorbent also shows the displacement of the amide I band after metal saturation, i.e., a shift from 1660 to 1640, 1642, and 1635 cm^{-1} after Nd^{3+}, Sc^{3+}, and Fe^{3+} saturation,

https://dx.doi.org/10.1021/acsami.0c16282
ACS Appl. Mater. Interfaces 2020, 12, 57003−57016

respectively (Figure 10b). However, the shift of the amide II band observed varies significantly according to the metal ion. For instance, a strong shift toward lower wavenumbers was observed for Nd^{3+}-modified materials, while Sc^{3+}- or Fe^{3+}-loaded samples either did not show any displacement in this region (Sc^{3+}) or displayed a shift toward higher wavenumbers (Fe^{3+}). The shift toward lower frequencies of amide I and amide II bands for the Nd-loaded material may indicate that the amide oxygen atom is a coordination center for lanthanides.[63] On the other hand, the shift toward lower frequencies of the carbonyl band after Sc^{3+} or Fe^{3+} saturation, jointly with a shift toward higher frequencies of the amide II band, could suggest that the amide nitrogen atom acts as a coordination site for these elements.[63] Further, upon metal loading, the O−H/N−H stretching region, 3700−3200 cm^{-1}, also changed and the broad band is more pronounced for Sc-loaded materials, suggesting the presence of coordinated water molecules in the metal coordination sphere. The shift of the amide I band toward lower wavenumbers was also observed in the case of KIT-6-N-DGA after loading different metal ions, i.e., shift from 1660 cm^{-1} to 1642 (Eu^{3+}), 1639 (Sc^{3+}), and 1635 cm^{-1} (Fe^{3+}) (Figure 10c). Upon metal loading, only KIT-6-N-DGA-Eu displayed a movement of the amide II band toward lower wavenumbers, indicating that the amide oxygen atom possibly reacts as a coordination center for lanthanides.[63−65] Moreover, the highest change of amide I/amide II band positions for the Eu^{3+}-modified material can suggest that KIT-6-N-DGA has a greater affinity toward Eu than other metals, i.e., Sc^{3+} or Fe^{3+}. Moreover, Sc- and Fe-loaded sorbents showed either a lack or a very small shift (+4 cm^{-1}) of the amide II band. The spectra of Sc- and Fe-loaded KIT-6-N-DGA samples display a more pronounced O−H region, implying the presence of water molecules in the inner coordination sphere. In contrast, this area stays unchanged after Eu^{3+} saturation.

Furthermore, the interactions between silica-based sorbents and loaded metal ions were probed by XPS, and the characteristic binding energies (BEs) and XPS plots are given in Table S5 and in Figures S5−S7. Although XPS is a surface technique and penetration depth is a few nanometers, it can provide some useful indications concerning the chemical environment of large pore silicas bearing metal complexes. Furthermore, in our case, the nature of the first layers can also be considered as representative of the inner ones. Based on our results, it is evident that after metal modification, all carbon signals are shifted toward higher BE, in comparison to the pristine hybrid sorbents. This shift is due to the formation of metal complexes.[66−68] After metal complexation, new signals also appear in the nitrogen and oxygen BE regions. Depending on the loaded metal and grafted ligand, these signals are associated with different species. For instance, peaks with BE energies at 402 and 407 eV, appearing after Sc^{3+} loading, can be fitted with Sc 2p spectra: Sc $2p_{3/2}$ and Sc $2p_{1/2}$ peaks, with the intensity ratio of Sc $2p_{3/2}$ and Sc $2p_{1/2}$ peaks 2:1.[69] However, the peak with the BE around 407 eV can also be attributed to the nitrate species, as this value is close to the BE found in other nitrate salts: BE = 408.0 eV for $Ca(NO_3)_2$; BE = 407.3 eV for NH_4NO_3; BE = 407.2 eV for KNO_3; or BE = 407.5 eV for $Ba(NO_3)_2$.[70] Interestingly, the relative intensity of this signal depends on the metal loaded. For instance, in the case of Fe-modified samples, its intensity is very high, whereas REE-loaded samples show low (KIT-6-N-FDGA-Gd) or almost negligible (KIT-6-N-DGA-Eu, KIT-6-N-DOODA-Nd) peaks in this region, indicating a lack of nitrates in the coordination sphere. In addition, after Fe^{3+} loading, the O 1s signal (BE around 532 eV) shows a broadening, which could be due to the presence of nitrates. The O 1s peak with the binding energy of 530.0 eV is a typical O 1s peak of metal oxides that may even indicate the presence of some iron oxide. The XPS and FT-IR results of metal-modified sorbents indicate that complexation between rare earth ions and DGA-type ligands is mostly devoid of nitrates in the inner coordination sphere of the chelated metal ions. In that case, the ligands present on the surface, with or without water molecules, saturate the metal coordination sphere, preventing the binding of NO_3^- ions. Differently, the presence of nitrates in the Fe^{3+} coordination sphere is evident and may thus be associated with either a different extraction mechanism (e.g., presence of different extraction/adsorption centers) or a less favorable ligand-silica environment. Consequently, this observation can explain why the obtained sorbents displayed higher extraction capacity and selectivity toward REEs than other elements.[9,15,16,40]

4. CONCLUSIONS

In summary, three different DGA-based hybrid silica sorbents have been designed and tested for rare earth element extraction/purification. The immobilization of different DGA derivatives caused distinct and significant enhancement in the extraction capacity, i.e., the KIT-6-N-DGA sorbent shows a higher extraction capacity toward middle elements, in contrast to the KIT-6-N-DOODA material that displays preference toward heavier Ln and KIT-6-N-FDGA sorbents showing selectivity to scandium ions. Furthermore, depending on the grafted ligand and extracted element, different atoms/group of atoms could play the role of the extraction site, consequently indicating that different extraction mechanisms or different complexation preferences may occur on the surface. Based on the presented data, it can be suggested that the amide nitrogen atom is the main coordination center for the transition metals (Fe or Sc), while lanthanides are mostly bound to amide oxygen atoms. Diverse selectivity profiles may be related to differences in the size of the chelating angle, density of OH groups, or the ligand surface environment, which highlights the importance of a precise design and anchoring of the chelating ligand on the (nano)porous support. Moreover, grafted ligands may not form a perfect monolayer on the silica surface, consequently creating gaps between ligand molecules, allowing for metal−silica surface (silanols) interactions (i.e., van der Waals forces or ionic bonds with deprotonated SiOH groups), which in turn may play a significant role in the extraction process. In agreement with our previous study, we observed such interactions in the specific case of Sc-modified materials.[50] Sc ions interact with both the silica surface and the tethered ligand molecules. However, the high extraction capacity of Sc^{3+} ions may suggest that not only weak interactions, e.g., van der Waals or ionic bonds, participate in the extraction process but one may expect the formation of a covalent bond (Si−O−Sc) (i.e., strong interaction), which is a slow process (Sc-OH + Si-OH → Si−O−Sc + H_2O). Therefore, longer extraction experiments (i.e., batch conditions) show much higher Sc^{3+} uptake, whereas in a flow system (i.e., dynamic extraction) this trend is only slightly visible. On the other hand, it seems unlikely that such a process would occur as rapidly and easily with the lanthanides. The coordination complexes between elements with larger ionic

https://dx.doi.org/10.1021/acsami.0c16282
ACS Appl. Mater. Interfaces 2020, 12, 57003−57016

radius and silica hybrid materials are formed essentially through the ligand moieties, i.e., the carbonyls of the amide.

To summarize the origin of the selectivity of the differently functionalized sorbents, the following conclusions can be drawn: (1) iron ions may not be well-retained in the (organo)silica sorbents due to the presence of nitrates in the coordination sphere of the metal; (2) scandium seems to be preferentially retained in sorbents where a higher density/number of residual silanols is available on the pore surface; and (3) for ligands that cover the pore surface more uniformly (i.e., less available residual silanols), the lanthanide selectivity appears to be determined mostly by the chelating angle of the grafted ligand, leading ultimately to the possibility of increased separation factors among the elements of this series.

Overall, we could correlate the hybrid sorbent structures to the metal extraction profiles and establish the coordination modes based on several spectroscopic analyses of the materials, with and without loaded metals. Our investigation allowed us to understand the role of specific pore surface functional groups (e.g., O-donor, N-donor, silanol groups) in enhancing metal−sorbent interactions, which ultimately determines the metal adsorption selectivity. The obtained results will be important to further design highly selective sorbents (in terms of both new ligands and optimized solid supports) with the aim of obtaining single-metal selective adsorbents. For the application, it will be essential to transfer the ligand systems onto structured silica materials, such as monoliths or microspheres, with adjustable and interconnected (hierarchical) mesoporosity/macroporosity to overcome mass transport and permeability issues. Furthermore, stable sorbents with robust mechanical properties are essential also to maintain multiple extraction cycles and recycling capabilities in different conditions and media (e.g., pH, competing elements, aqueous, oil). Finally, it is important to note that although batch experiments allow for a good characterization of the sorbents and the identification of key parameters, they do not reflect exactly the real working performance of the material such as in nonequilibrated dynamic studies (e.g., flow-through column).

■ ASSOCIATED CONTENT

Supporting Information

The Supporting Information is available free of charge at https://pubs.acs.org/doi/10.1021/acsami.0c16282.

Detailed ligand synthesis procedures, nitrogen physisorption data (isotherms and respective pore size distributions), thermogravimetric data, detailed XPS results, ^{29}Si CP NMR results, and additional extraction chromatography data (Langmuir and Freundlich fitting plots) (PDF)

■ AUTHOR INFORMATION

Corresponding Author

Justyna Florek − *Department of Inorganic Chemistry - Functional Materials, Faculty of Chemistry, University of Vienna, 1090 Vienna, Austria;* orcid.org/0000-0001-8891-2474; Phone: +43 1 4277 52903; Email: justyna.florek@univie.ac.at

Authors

Dominic Larivière − *Department of Chemistry, Université Laval, Québec, QC G1V 0A6, Canada; Centre en Catalyse et Chimie Verte (C3V) Université Laval, Québec, QC G1V 0A6, Canada;* orcid.org/0000-0003-1860-1181

Hanspeter Kählig − *Department of Organic Chemistry, Faculty of Chemistry, University of Vienna, 1090 Vienna, Austria*

Sonia L. Fiorilli − *Dipartimento di Scienza Applicata e Tecnologia, Politecnico di Torino, 10129 Torino, Italy*

Barbara Onida − *Dipartimento di Scienza Applicata e Tecnologia, Politecnico di Torino, 10129 Torino, Italy*

Frédéric-Georges Fontaine − *Department of Chemistry and Canada Research Chair in Green Catalysis and Metal-Free Processes, Université Laval, Québec, QC G1V 0A6, Canada; Centre en Catalyse et Chimie Verte (C3V) Université Laval, Québec, QC G1V 0A6, Canada;* orcid.org/0000-0003-3385-0258

Freddy Kleitz − *Department of Inorganic Chemistry - Functional Materials, Faculty of Chemistry, University of Vienna, 1090 Vienna, Austria;* orcid.org/0000-0001-6769-4180

Complete contact information is available at: https://pubs.acs.org/10.1021/acsami.0c16282

Notes

The authors declare no competing financial interest.

■ ACKNOWLEDGMENTS

The authors (J.F., H.K., F.K.) acknowledge the funding support of the University of Vienna (Austria). The authors also wish to thank the Fonds de Recherche Québécois Nature et Technologies (FRQNT, Grant No. 174923-2013), National Sciences and Engineering Research Council of Canada (NSERC, Grant No. STPGP-463032-2014), and the Government of Quebec, Ministère des Relations Internationales et de la Francophonie, and the Consulat Général d'Italie à Montréal for funding in the exchange program "VIII^{e} Réunion de la Sous-commission Mixte de Québec-Italie (Coopération 2013−2015)" for financial support. The authors thank Professor Ryong Ryoo (KAIST and Institute for Basic Science, Daejeon, Republic of Korea) for providing the TEM and XRD analyses. J.F. acknowledges Marco Pavani for help with FT-IR measurements in Politecnico di Torino (Italy).

■ REFERENCES

(1) Wang, W.; Pranolo, Y.; Cheng, C. Y. Metallurgical Processes for Scandium Recovery from Various Resources: A Review. *Hydrometallurgy* **2011**, *108*, 100−108.

(2) Maes, S.; Zhuang, W.-Q.; Rabaey, K.; Alvarez-Cohen, L.; Hennebel, T. Concomitant Leaching and Electrochemical Extraction of Rare Earth Elements from Monazite. *Environ. Sci. Technol.* **2017**, *51*, 1654−1661.

(3) Ritter, S. K. *A Whole New World for Rare Earths*; C&EN, 2017.

(4) Jordens, A.; Cheng, Y. P.; Waters, K. E. A Review of the Beneficiation of Rare Earth Element Bearing Minerals. *Miner. Eng.* **2013**, *41*, 97−114.

(5) Sholl, D. S.; Lively, R. P. Seven Chemical Separations to Change the World. *Nature* **2016**, *532*, 435−437.

(6) Cheisson, T.; Schelter, E. J. Rare Earth Elements: Mendeleev's Bane, Modern Marvels. *Science* **2019**, *363*, 489−493.

(7) Alonso, E.; Sherman, A. M.; Wallington, T. J.; Everson, M. P.; Field, F. R.; Roth, R.; Kirchain, R. E. Evaluating Rare Earth Element Availability: A Case with Revolutionary Demand from Clean Technologies. *Environ. Sci. Technol.* **2012**, *46*, 3406−3414.

(8) Zheng, X.; Zhang, F.; Liu, E.; Xu, X.; Yan, Y. Efficient Recovery of Neodymium in Acidic System by Free-Standing Dual-Template

Docking Oriented Ionic Imprinted Mesoporous Films. *ACS Appl. Mater. Interfaces* **2017**, *9*, 730−739.
(9) Hu, Y.; Misal Castro, L. C.; Drouin, E.; Florek, J.; Kählig, H.; Larivière, D.; Kleitz, F.; Fontaine, F.-G. Size-Selective Separation of Rare Earth Elements Using Functionalized Mesoporous Silica Materials. *ACS Appl. Mater. Interfaces* **2019**, *11*, 23681−23691.
(10) Wilfong, W. C.; Kail, B. W.; Bank, T. L.; Howard, B. H.; Gray, M. L. Recovering Rare Earth Elements from Aqueous Solution with Porous Amine−Epoxy Networks. *ACS Appl. Mater. Interfaces* **2017**, *9*, 18283−18294.
(11) Zheng, X.; Zhang, F.; Liu, E.; Xu, X.; Yan, Y. Efficient Recovery of Neodymium in Acidic System by Free-Standing Dual-Template Docking Oriented Ionic Imprinted Mesoporous Films. *ACS Appl. Mater. Interfaces* **2017**, *9*, 730−739.
(12) Uda, T.; Jacob, K. T.; Hirasawa, M. Technique for Enhanced Rare Earth Separation. *Science* **2000**, *289*, 2326−2329.
(13) Kumar, B. N.; Radhika, S.; Reddy, B. R. Solid−Liquid Extraction of Heavy Rare-Earths from Phosphoric Acid Solutions Using Tulsion CH-96 and T-PAR Resins. *Chem. Eng. J.* **2010**, *160*, 138−144.
(14) Dave, S. R.; Kaur, H.; Menon, S. K. Selective Solid-Phase Extraction of Rare Earth Elements by the Chemically Modified Amberlite XAD-4 Resin with Azacrown Ether. *React. Funct. Polym.* **2010**, *70*, 692−698.
(15) Florek, J.; Mushtaq, A.; Larivière, D.; Cantin, G.; Fontaine, F.-G.; Kleitz, F. Selective Recovery of Rare Earth Elements Using Chelating Ligands Grafted on Mesoporous Surfaces. *RSC Adv.* **2015**, *5*, 10378−103789.
(16) Florek, J.; Chalifour, F.; Bilodeau, F.; Larivière, D.; Kleitz, F. Nanostructured Hybrid Materials for the Selective Recovery and Enrichment of Rare Earth Elements. *Adv. Funct. Mater.* **2014**, *24*, 2668−2676.
(17) Hu, Y.; Drouin, E.; Larivière, D.; Kleitz, F.; Fontaine, F.-G. Highly Efficient and Selective Recovery of Rare Earth Elements Using Mesoporous Silica Functionalized by Preorganized Chelating Ligands. *ACS Appl. Mater. Interfaces* **2017**, *9*, 38584−38593.
(18) Ashour, R. M.; Samouhos, M.; Legaria, E. P.; Svärd, M.; Högblom, J.; Forsberg, K.; Palmlöf, M.; Kessler, V. G.; Seisenbaeva, G. A.; Rasmuson, ÅC. DTPA-Functionalized Silica Nano- and Microparticles for Adsorption and Chromatographic Separation of Rare Earth Elements. *ACS Sustainable Chem. Eng.* **2018**, *6*, 6889−6900.
(19) Callura, J. C.; Perkins, K. M.; Noack, C. W.; Washburn, N. R.; Dzombak, D. A.; Karamalidis, K. Selective Adsorption of Rare Earth Elements onto Functionalized Silica Particles. *Green Chem.* **2018**, *20*, 1515−1526.
(20) Li, X.-Z.; Zhou, L.-P.; Yan, L.-L.; Dong, Y.-M.; Bai, Z.-L.; Sun, X.-Q.; Diwu, J.; Wang, S.; Bunzli, J.-C.; Sun, Q.-F. A Supramolecular Lanthanide Separation Approach Based on Multivalent Cooperative Enhancement of Metal ion Selectivity. *Nat. Commun.* **2018**, *9*, No. 547.
(21) Yin, X.; Wang, Y.; Bai, X.; Wang, Y.; Chen, L.; Xiao, C.; Diwu, J.; Du, S.; Chai, Z.; Albrecht-Schmitt, T. E.; Wang, S. Rare Earth Separations by Selective Borate Crystallization. *Nat. Commun.* **2017**, *8*, No. 14438.
(22) Jańczewski, D.; Reinhoudt, D. N.; Verboom, W.; Hill, C.; Allignol, C.; Duchesne, M.-T. Tripodal Diglycolamides as Highly Efficient Extractants for f-elements. *New J. Chem.* **2008**, *32*, 490−495.
(23) Cotruvo, J. A., Jr.; Featherston, E. R.; Mattocks, J. A.; Ho, J. V.; Laremore, T. N. Lanmodulin: A Highly Selective Lanthanide-Binding Protein from a Lanthanide-Utilizing Bacterium. *J. Am. Chem. Soc.* **2018**, *140*, 15056−15061.
(24) Florek, J.; Giret, S.; Juère, E.; Larivière, D.; Kleitz, F. Functionalization of Mesoporous Materials for Lanthanide and Actinide Extraction. *Dalton Trans.* **2016**, *45*, 14832−14854.
(25) Matloka, K.; Gelis, A.; Regalbuto, M.; Vandegrift, G.; Scott, M. J. Highly Efficient Binding of Trivalent f-elements from Acidic Media with a C_3-symmetric Tripodal Ligand Containing Diglycolamide Arms. *Dalton Trans.* **2005**, 3719−3721.
(26) Kannan, S.; Moody, M. A.; Barnes, C. L.; Duval, P. B. Lanthanum(III) and Uranyl(VI) Diglycolamide Complexes: Synthetic Precursors and Structural Studies Involving Nitrate Complexation. *Inorg. Chem.* **2008**, *47*, 4691−4695.
(27) Leoncini, A.; Huskens, J.; Verboom, W. Ligands for f-element Extraction Used in the Nuclear Fuel Cycle. *Chem. Soc. Rev.* **2017**, *46*, 7229−7273.
(28) Armelao, L.; Dell'Amico, D. B.; Bellucci, L.; Bottaro, G.; Di Bari, L.; Labella, L.; Marchetti, F.; Samaritani, S.; Zinna, F. Circularly Polarized Luminescence of Silica-Grafted Europium Chiral Derivatives Prepared through a Sequential Functionalization. *Inorg. Chem.* **2017**, *56*, 7010−7018.
(29) Housecroft, C.; Sharpe, A. G. *Inorganic Chemistry*, 3rd ed.; Prentice Hall: Essex, England, 2007; Chapter 25.
(30) Lefrancois Perreault, L.; Giret, S.; Gagnon, M.; Florek, J.; Larivière, D.; Kleitz, F. Functionalization of Mesoporous Carbon Materials for Selective Separation of Lanthanides under Acidic Conditions. *ACS Appl. Mater. Interfaces* **2017**, *9*, 12003−12012.
(31) Liu, C. C.; Maciel, G. E. The Fumed Silica Surface: A Study by NMR. *J. Am. Chem. Soc.* **1996**, *118*, 5103−5119.
(32) Trébosc, J.; Wiench, J. W.; Huh, S.; Lin, V. S. Y.; Pruski, M. Solid-state NMR Study of MCM-41-type Mesoporous Silica Nanoparticles. *J. Am. Chem. Soc.* **2005**, *127*, 3057−3068.
(33) Brown, S. P. Applications of high resolution ^{1}H solid-state NMR. *Solid State NMR* **2012**, *41*, 1−27.
(34) Faulkner, R. A.; DiVerdi, J. A.; Yang, Y.; Kobayashi, T.; Maciel, G. E. The Surface of Nanoparticle Silicon as Studied by Solid-State NMR. *Materials* **2013**, *6*, 18−46.
(35) Jedlicka, S. J.; Rickus, J. L.; Zemlyanov, D. Y. Surface Analysis by X-ray Photoelectron Spectroscopy of Sol-Gel Silica Modified with Covalently Bound Peptides. *J. Phys. Chem. B* **2007**, *111*, 11850−11857.
(36) Soulé, S.; Allouche, J.; Dupin, J. C.; Courrèges, C.; Plantier, F.; Ojo, W.-S.; Coppel, Y.; Nayral, C.; Delpech, F.; Martinez, H. Thermoresponsive Gold Nanoshell@Mesoporous Silica Nano-Assemblies: an XPS/NMR Survey. *Phys. Chem. Chem. Phys.* **2015**, *17*, 28719−28728.
(37) Ide, M.; El-Roz, M.; De Canck, E.; Vicente, A.; Planckaert, T.; Bogaerts, T.; Van Driessche, I.; Lynen, F.; Van Speybroeck, V.; Thybault-Starzyk, F.; Van Der Voort, P. Quantification of Silanol Sites for the Most Common Mesoporous Ordered Silicas and Organosilicas: Total Versus Accessible Silanols. *Phys. Chem. Chem. Phys.* **2013**, *15*, 642−650.
(38) Shusterman, J. A.; Mason, H.; Bruchet, A.; Zavarin, M.; Kersting, A. B.; Nitsche, H. Analysis of Trivalent Cation Complexation to Functionalized Mesoporous Silica Using Solid-State NMR Spectroscopy. *Dalton Trans.* **2014**, *43*, 16649−16658.
(39) Ali, S. M.; Pahan, S.; Bhattacharyya, A.; Mohapatra, P. K. Complexation Thermodynamics of Diglycolamidewith f-elements: Solvent Extraction and Density Functional Theory Analysis. *Phys. Chem. Chem. Phys.* **2016**, *18*, 9816−9828.
(40) Hopkins, P. D.; Mastren, T.; Florek, J.; Copping, R.; Brugh, M.; John, K. D.; Nortier, M. F.; Birnbaum, E. R.; Kleitz, F.; Fassbender, M. E. Synthesis and Radiometyric Evaluation of Diglycolamide Functionalized Mesoporous Slica for the Chromatographic Separation of Actinides Th, Pa and U. *Dalton Trans.* **2018**, *47*, 5189−5195.
(41) Lebed, P. J.; Savoie, J.-D.; Florek, J.; Bilodeau, F.; Larivière, D.; Kleitz, F. Large Pore Mesostructured Organosilica-Phosphonate Hybrids as Highly Efficient and Regenerable Sorbents for Uranium Sequestration. *Chem. Mater.* **2012**, *24*, 4166−4176.
(42) Kleitz, F.; Choi, S. H.; Ryoo, R. Cubic Ia3d Large Mesoporous Silica: Synthesis and Replication to Platinum Nanowires, Carbon Nanorods and Carbon Nanotubes. *Chem. Commun.* **2003**, 2136−2137.
(43) Kleitz, F.; Bérubé, F.; Guillet-Nicolas, R.; Yang, C.-M.; Thommes, M. Probing Adsorption, Pore Condensation, and Hysteresis Behavior of Pure Fluids in Three-Dimensional Cubic Mesoporous KIT-6 Silica. *J. Phys. Chem. C* **2010**, *114*, 9344−9355.

https://dx.doi.org/10.1021/acsami.0c16282
ACS Appl. Mater. Interfaces 2020, 12, 57003−57016

(44) Kim, T.-W.; Kleitz, F.; Paul, B.; Ryoo, R. MCM-48-like Large Mesoporous Silicas with Tailored Pore Structure: Facile Synthesis Domain in a Ternary Triblock Copolymer−Butanol−Water System. *J. Am. Chem. Soc.* **2005**, *127*, 7601−7610.
(45) Wang, G. P.; Chang, T. C.; Hong, Y. S.; Chui, Y. S. Dynamics of Novel Hydrogen-Bonded Acidic Fluorinated Poly(amide-imide-silica) Hybrids Studied by Solid-State NMR. *Polymer* **2002**, *43*, 2191−2000.
(46) Peng, H.; Alemany, L. B.; Margrave, J. L.; Khabashesku, V. N. Sidewall Carboxylic Acid Functionalization of Single-Walled Carbon Nanotubes. *J. Am. Chem. Soc.* **2003**, *125*, 15174−15182.
(47) Guan, S.; Inagaki, S.; Ohsuna, T.; Terasaki, O. Hybrid Ethane−Siloxane Mesoporous Materials with Cubic Symmetry. *Microporous Mesoporous Mater.* **2001**, *44*−*45*, 165−172.
(48) Fowler, C. E.; Burkett, S. L.; Mann, S. Synthesis and Characterization of Ordered Organo−Silica−Surfactant Mesophases with Functionalized MCM-41-type Architecture. *Chem. Commun.* **1997**, 1769−1770.
(49) Marcoux, L.; Florek, J.; Kleitz, F. Critical Assessment of the Base Catalysis Properties of Amino-Functionalized Mesoporous Polymer-SBA-15 Nanocomposites. *Appl. Catal., A* **2015**, *504*, 493−503.
(50) Giret, S.; Hu, Y.; Masoumifard, N.; Boulanger, J. F.; Juère, E.; Kleitz, F.; Larivière, D. Selective Separation and Preconcentration of Scandium with Mesoporous Silica. *ACS Appl. Mater. Interfaces* **2018**, *10*, 448−457.
(51) Hu, Y.; Giret, S.; Meinusch, R.; Han, J.; Fontaine, F.-G.; Kleitz, F.; Larivière, D. Selective Separation and Preconcentration of Th(iv) Using Organo-Functionalized, Hierarchically Porous Silica Monoliths. *J. Mater. Chem. A* **2019**, *7*, 289−302.
(52) Lunn, J. D.; Shantz, D. F. Peptide Brush—Ordered Mesoporous Silica Nanocomposite Materials. *Chem. Mater.* **2009**, *21*, 3638−3648.
(53) Zecchina, A.; Geobaldo, F.; Spoto, G.; Bordiga, S.; Ricchiardi, G.; Buzzoni, R.; Petrini, G. FTIR Investigation of the Formation of Neutral and Ionic Hydrogen-Bonded Complexes by Interaction of H-ZSM-5 and H-Mordenite with CH_3CN and H_2O: Comparison with the H-NAFION Superacidic System. *J. Phys. Chem. A* **1996**, *100*, 16584−16599.
(54) Socrates, G. *Infrared and Raman Characteristic Group Frequencies: Tables and Chats*, 3rd ed.; John Wiley & Sons, Ltd: West Sussex, England, 2001.
(55) Singh, D. P.; Pratap, S.; Gupta, S. K.; Butcher, R. J. Structural and Spectral Speciation on Methyl 2-(3-(furan-2-carbonyl)-thioureido)benzoate: A Comparative Experimental and Theoretical Study. *J. Mol. Struct.* **2013**, *1048*, 500−509.
(56) Vieira, R. S.; Oliveira, M. L. M.; Guibal, E.; Rodríguez-Castellón, E.; Beppu, M. M. Copper, Mercury and Chromium Adsorption on Natural and Crosslinked Chitosan films: An XPS Investigation of Mechanism. *Colloids Surf., A* **2011**, *374*, 108−114.
(57) Shan, M.; Kang, H.; Xu, Z.; Li, N.; Jing, M.; Hu, Y.; Teng, K.; Qian, X.; Shi, J.; Liu, L. Decreased Cross-Linking in Interfacial Polymerization and Heteromorphic Support Between Nanoparticles: Towards High-Water and Low-Solute Flux of Hybrid Forward Osmosis Membrane. *J. Colloid Interface Sci.* **2019**, *548*, 170−183.
(58) Zhang, W.; Avdibegović, D.; Koivula, R.; Hatanpää, T.; Hietala, S.; Regadío, M.; Binnemans, K.; Harjula, R. Titanium alkylphosphate functionalised mesoporous silica for enhanced uptake of rare-earth ions. *J. Mater. Chem. A* **2017**, *5*, 23805−23814.
(59) Horwitz, E. P.; McAlister, D. R.; Bond, A. H.; Barrans, R. E., Jr. Novel Extraction of Chromatographic Resins Based on Tetraalkyldiglycolamides: Characterization and Potential Applications. *Solvent Extr. Ion Exch.* **2005**, *23*, 319−344.
(60) Zhang, W.; Hietala, S.; Khriachtchev, L.; Hatanpää, T.; Doshi, B.; Koivula, R. Intralanthanide Separation on Layered Titanium (IV)Organophosphate Materials via a Selective Transmetalation Process. *ACS Appl. Mater. Interfaces* **2018**, *10*, 22083−22093.
(61) Roosen, J.; Van Roosendael, S.; Rao Borra, C.; Van Gerven, T.; Mullensc, S.; Binnemans, K. Recovery of Scandium from Leachates of Greekbauxite Residue by Adsorption on Functionalized Chitosan−Silica Hybrid Materials. *Green Chem.* **2016**, *18*, 2005−2013.
(62) Liu, H.; Yang, F.; Zheng, Y.; Kang, J.; Qu, J.; Chen, J. P. Improvement of Metal Adsorption onto Chitosan/Sargassum sp. Composite Sorbent by an Innovative Ion-Imprint Technology. *Water Res.* **2011**, *45*, 145−154.
(63) Reilly, S. D.; Gaunt, A. J.; Scott, B. L.; Modolo, G.; Iqbal, M.; Verboom, W.; Sarsfield, M. J. Plutonium(iv) Complexation by Diglycolamideligands—Coordination Chemistry Insight Into TODGA-based Actinide Separations. *Chem. Commun.* **2012**, *48*, 9732−9734.
(64) Deb, S. B.; Gamare, J. S.; Kannan, S.; Drew, M. G. Uranyl(VI) and Lanthanum(III) Thio-Diglycolamides Complexes: Synthesis and Structural Studies Involving Nitrate Complexation. *Polyhedron* **2009**, *28*, 2673−2678.
(65) Nelwamondo, A. N.; Eve, D. J.; Watkins, G. M.; Brown, M. E. Thermal and Structural Studies of Amide Complexes of Transition Metal(II) Chlorides. I: Stoichiometry. *Thermochim. Acta* **1998**, *318*, 165−175.
(66) Grissa, R.; Abramova, A.; Tambio, S. J.; Lecuyer, M.; Deschamps, M.; Fernandez, V.; Moreau, P. Thermomechanical Polymer Binder Reactivity with Positive Active Materials for Li Metal Polymer and Li-Ion Batteries: An XPS and XPS Imaging Study. *ACS Appl. Mater. Interfaces* **2019**, *11*, 18368−18376.
(67) Zhang, C.; Li, X.; Jiang, Z.; Zhang, Y.; Wen, T.; Fang, M.; Wang, X. Selective Immobilization of Highly Valent Radionuclides by Carboxyl Functionalized Mesoporous Silica Microspheres: Batch, XPS, and EXAFS Analyses. *ACS Sustainable Chem. Eng.* **2018**, *6*, 15644−15652.
(68) Qi, X. H.; Du, K. Z.; Feng, M. L.; Gao, Y. J.; Huang, X. Y.; Kanatzidis, M. G. Layered A2Sn3S7·1.25H2O (A = Organic Cation) as Efficient Ion-Exchanger for Rare Earth Element Recovery. *J. Am. Chem. Soc.* **2017**, *139*, 4314−4317.
(69) Biesinger, M. C.; Lau, L. W. M.; Gerson, A. R.; Smart, R. S. C. Resolving Surface Chemical States in XPS Analysis of First Row Transition Metals, Oxides and Hydroxides: Sc, Ti, V, Cu and Zn. *Appl. Surf. Sci.* **2010**, *257*, 887−898.
(70) Baltrusaitis, J.; Jayaweera, P. M.; Grassian, V. H. XPS Study of Nitrogen Dioxide Adsorption on Metal Oxide Particle Surfaces Under Different Environmental Conditions. *Phys. Chem. Chem. Phys.* **2009**, *11*, 8295−8305.

https://dx.doi.org/10.1021/acsami.0c16282
ACS Appl. Mater. Interfaces 2020, 12, 57003−57016